Yeast Tripartite Biosensors Sensitive to Protein Stability and Aggregation Propensity

Veronika Sachsenhauser, Xiexiong Deng,[#] Hyun-hee Kim,[#] Maja Jankovic, and James C.A. Bardwell*

Cite This: *ACS Chem. Biol.* 2020, 15, 1078−1088

Read Online

ACCESS | 📊 Metrics & More | 📰 Article Recommendations | 🔵 Supporting Information

ABSTRACT: In contrast to the myriad approaches available to study protein misfolding and aggregation *in vitro*, relatively few tools are available for the study of these processes in the cellular context. This is in part due to the complexity of the cellular environment which, for instance, interferes with many spectroscopic approaches. Here, we describe a tripartite fusion approach that can be used to assess *in vivo* protein stability and solubility in the cytosol of *Saccharomyces cerevisiae*. Our biosensors contain tripartite fusions in which a protein of interest is inserted into antibiotic resistance markers. These fusions act to directly link the aggregation susceptibility and stability of the inserted protein to antibiotic resistance. We demonstrate a linear relationship between the thermodynamic stabilities of variants of the model folding protein immunity protein 7 (Im7) fused into the resistance markers and their antibiotic resistance readouts. We also use this system to investigate the *in vivo* properties of the yeast prion proteins Sup35 and Rnq1 and proteins whose aggregation is associated with some of the most prevalent neurodegenerative misfolding disorders, including peptide amyloid beta 1−42 (Aβ42), which is involved in Alzheimer's disease, and protein α-synuclein, which is linked to Parkinson's disease.
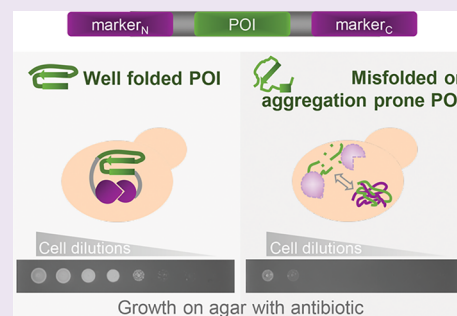
INTRODUCTION

Protein misfolding and aggregation are hallmarks of many disease states, ranging from disorders that affect the central nervous system to those that lead to amyloidosis in the liver.[1] Although the chemical identity and misfolding state of the proteins involved in these diseases are unique, these proteopathies are generally characterized by the adoption of aberrant protein conformations, which often seed aggregation or amyloid formation. In some cases, these conformational changes are toxic, and in other cases, they lead to disruption of the protein's function.

Predicting *in vivo* protein stability or aggregation propensity based just on the protein's sequence, structure, or *in vitro* properties is a hit and miss affair. This is in part because the cellular environment is very crowded and contains a variety of factors that can affect protein folding, including molecular chaperones, ligands, and protein quality control machinery. Additionally, the cell's changing physical and chemical properties, including its redox state, temperature, and the formation of transient biomolecular condensation phases, can impact protein solubility.[2,3] Moreover, cellular aggregates can be complex and differ from one another in their size, conformation, and constituents. Considering these complex factors highlights the urgent need to establish generalizable methods that allow one to assess the actual *in vivo* folding state of proteins, particularly of disease-related proteins.

Budding yeast *Saccharomyces cerevisiae* has proven to be a valuable model organism to study protein folding. It is cost-efficient, easy to genetically manipulate, and amenable to high-throughput screens, and thus provides a facile eukaryotic context for deciphering fundamental molecular processes involved in complex *in vivo* protein misfolding phenomena.[4] In addition, several yeast models have allowed for the screening of cellular and chemical factors affecting the stability or aggregation propensity of disease-associated proteins.[5−7]

Several indirect, potentially generalizable methods to determine the folding and aggregation status of proteins in yeast have been engineered. Fluorescent tagging has been widely used to detect a protein's spatiotemporal localization and aggregation propensity.[8−14] This method has been shown to effectively read-out protein solubility, though in some cases fluorescent tags enhance solubility, can cause some false-positive results due to proteolytic cleavage products, or can be influenced by fused amyloidogenic sequences.[9,15,16] In addition, other fusion-based approaches that link protein solubility to yeast growth have been devised.[17,18] Other commonly used approaches to study the aggregation propensity of neuro-pathogenic proteins in yeast utilize overexpression-induced cytotoxicity as a readout.[6,11] These assays have greatly contributed to our general understanding of protein misfolding

in the cell. It is noteworthy that the acute toxicity that results from high levels of overexpression may occur via mechanisms different than those of the long-term toxicity often associated with neurodegenerative diseases.[19,20] In addition, high levels of overexpression can cause sequestration of native and non-native binding partners and lead to transport into non-native cellular compartments.[21] Although valuable insights have been gained from the series of yeast models that have emerged, different experimental models can generate different and sometimes contradictory results. For instance, the PICALM protein has been identified both as a suppressor and an enhancer of Aβ cytotoxicity.[6,14]

Because biosensors are based on different underlying principles, their results are complementary to each other. Inherent limitations in existing protein folding and aggregation sensors continue to drive the development of new methods based on different underlying principles. Recent fluorescence resonance energy transfer-based approaches or methods based on modular, transcriptional reporter outputs have helped generate tools that appear quantitative and suitable for high-throughput studies.[22,23] Here, we describe the development of a biosensor platform that links protein stability and aggregation propensity to an antibiotic resistance readout in yeast. Our goal is to provide a versatile tool that allows us to determine the *in vivo* stability of proteins of interest and interrogate stability-related phenomena in yeast.

■ RESULTS AND DISCUSSION

Development of Tripartite Folding Biosensors in *S. cerevisiae*. To study protein stability *in vivo*, we developed tripartite biosensors that link protein stability to antibiotic resistance.[24,25] The tripartite biosensor design comprises the fusion of a protein of interest into the middle of a genetic marker protein via flexible linkers (Figure 1a). We hypothesize that if the protein of interest folds well and remains stable, the two fused marker halves will come together, efficiently fold up, and thus confer high levels of antibiotic resistance (Figure 1b). However, if the protein of interest is thermodynamically unstable and therefore prone to proteolysis or aggregation, the entire tripartite fusion will become susceptible to degradation or aggregation, either of which will render it nonfunctional or only partially functional. Therefore, we reason that the antibiotic resistance conferred by the tripartite fusion should serve as a direct readout of the stability and solubility of the fused protein *in vivo*.

Previously, we developed cytosolic tripartite biosensors based on two different broad-spectrum antibiotic resistance markers.[25] One, conferring resistance to the antibiotic G418, was based on the marker protein aminoglycoside-3′-phosphotransferase (APH), and the other, effective against the antibiotic nourseothricin (NTC), was based on nourseothricin N-acetyl transferase (NAT). The APH- and NAT-based tripartite biosensors worked effectively in the *Escherichia coli* cytosol but exhibited comparatively low sensitivity when used in yeast.[25]

To improve the biosensors' readouts for *S. cerevisiae*, we extensively re-engineered the sensors to increase their sensitivity and extend their dynamic range. This reengineering involved altering the tripartite biosensors' expression levels by changing gene dosage, optimizing the APH fusion codon, adjusting the incubation temperature, fine-tuning the insertion site within the NAT resistance protein, and altering the yeast strain background (see Supplementary Figures 1, 2 and Methods for details). Our choice of a relatively long 40 glycine—serine-rich linker (GS
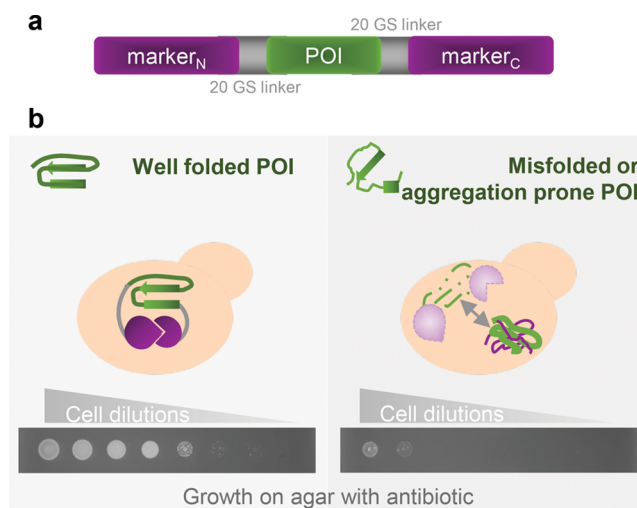

Figure 1. Design of a tripartite biosensor to study protein stability in yeast. (a) Schematic diagram of the tripartite fusion system. The protein of interest (green) is inserted into an antibiotic resistance marker protein (purple) with flexible, glycine—serine-rich linkers (gray) as part of a tripartite fusion. marker$_N$ and marker$_C$: N- and C-terminal half, respectively, of a split antibiotic resistance marker protein; POI: protein of interest; GS linker: glycine—serine-rich linker with a total length of 40 amino acid; 20 amino acids of the GS linker is fuse to each terminus of the POI and the respective marker half. (b) How the tripartite biosensor works: If the POI is folded properly or has low aggregation propensity, the tripartite fusion should remain intact and confer high levels of antibiotic resistance. However, poor folding or poor solubility of the test protein should result in increased susceptibility to proteolysis or aggregation in the yeast cytosol, which will in turn lead to lower antibiotic resistance. Therefore, the level of antibiotic resistance of yeast cells may be directly correlated to the folding or solubility of the inserted protein. Antibiotic resistance levels of yeast cells expressing the tripartite fusion can be quantified by a serial dilution spotting assay on agar media supplemented with antibiotic.

linker) (Figure 1, and Methods for details) between the marker halves was driven by the perceived need to be able to span the distance from the N- to C-termini of inserted proteins.[24,25] Our GS linker should be able to effectively stretch over the N- and C-termini of globular proteins (approximated as a sphere) up to 100 kDa in size, assuming the N- and C-termini are at the opposite poles of the sphere.[26,27] Elongated proteins, particularly highly extended ones, will be less able to be spanned. In previous work, we could already show that these particular GS-rich linker lengths are optimal for the relationship between antibiotic resistance to thermodynamic stability of the test protein fused in the tripartite system.[24]

To validate our revised tripartite design for yeast, we first inserted variants of Im7 that exhibit varying levels of thermodynamic stability. The rationale was that the *in vitro* thermodynamic stability of Im7 and other test proteins has been shown to be a key determinant of the level of antibiotic resistance displayed by tripartite fusions,[24,25] so we should expect similar results with our new designs.

Expression of the APH tripartite biosensors that just contained a 40-residue GS-rich linker between the marker halves, or 39-residue GS-rich linker for NAT-tripartite biosensors, conferred high levels of antibiotic resistance and served as a positive control.[25] To quantitatively describe the differences in antibiotic sensitivity observed in spot assays, we used the titration data to calculate the minimum inhibitory concentration (MIC) of antibiotic that inhibited cell growth for
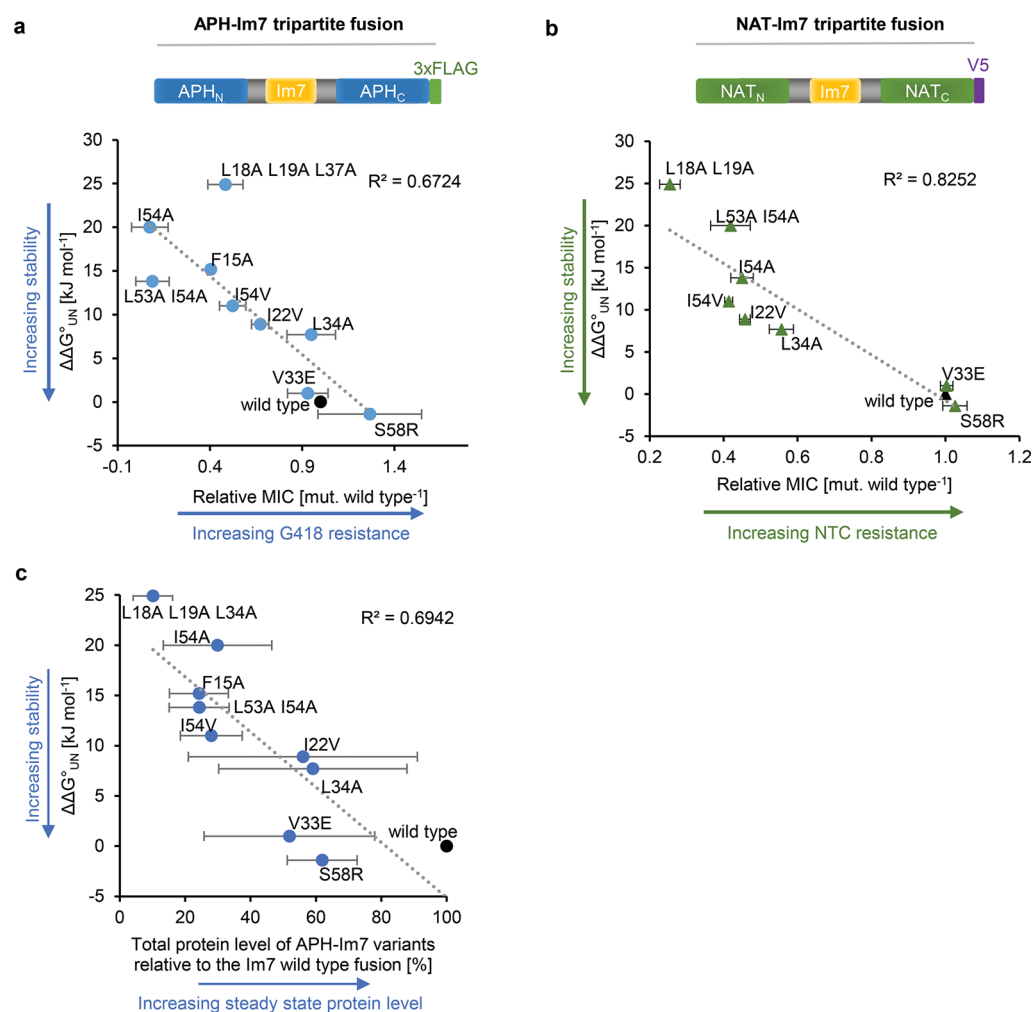
Figure 2. Stability of Im7 variants correlates with antibiotic resistance. Thermodynamically destabilized variants and a stabilized variant of Im7 (S58R) were inserted into (a) APH or (b) NAT via flexible linkers. The level of antibiotic resistance for cells expressing the corresponding fusion constructs was determined as the MIC in serial dilution spot assays as described in Supplementary Figure 2. The average MIC for G418 or NTC, respectively, relative to WT Im7, is plotted against the change in the free energy of unfolding, $\Delta\Delta G°_{UN}$, where $\Delta\Delta G°_{UN} = \Delta G°_{UN}$ (mutant) $- \Delta G°_{UN}$ (WT). The $\Delta G°_{UN}$ values for Im7 variants were determined by *in vitro* equilibrium urea denaturation.[24,28−30] (c) Thermodynamic stabilities of Im7 variants were plotted against the total protein level of APH-Im7 variant fusions relative to −Im7 WT fusions in *S. cerevisiae*. Protein levels were determined from lysates by immunoblotting against the FLAG epitope present on the C terminus of APH fusions and against glucose-6-phosphate dehydrogenase (G6PDH) as a loading control (Supplementary Figure 3). Experiments of panels a and c were performed in triplicate and of b in duplicate, and error bars indicate ±1 SD.

each tripartite variant relative to the Im7 wild-type (WT) insertion, as described previously.[24] For both the APH- and the NAT-based tripartite biosensors, we observed a good relationship between the *in vitro* thermodynamic stabilities determined by *in vitro* equilibrium urea denaturation of the tested Im7 variants[24,28−30] and their relative MICs (Figure 2a, b and Supplementary Figure 3), consistent with our previous findings for the Im7 tripartite system in *E. coli*[24,25] and first versions of the tripartite sensors in yeast.[25] The thermodynamic stabilities of these Im7 variants range from 24.9 to −1.4 kJ mol⁻¹, evidence that our yeast folding biosensors are sensitive at least over this range.

To assess whether the differences in Im7 thermodynamic stabilities are reflected in the steady state protein levels of the Im7 biosensor variants, we conducted quantitative Western blotting (Figure 2c and Supplementary Figure 3c, f). Levels in the total protein and soluble lysate fractions of APH-Im7 fusions showed an equally linear relationship with Im7 thermodynamic stabilities, leading us to conclude that the changes in steady state

levels are most likely due to *in vivo* proteolysis, an observation that is in keeping with the known close relationship between *in vivo* and *in vitro* stability.[24,31,32] We did not, however, observe a linear relationship between Im7 thermodynamic stabilities and protein levels for NAT-Im7, despite the strong correlation obtained between these stabilities and relative MIC values. Presumably, the NAT tripartite context may affect the solubility of the Im7 tripartite fusions, as has been commonly observed with other fusion proteins such as green fluorescent protein (GFP).[9] However, the folding status of fused Im7 variants still apparently determines the complementation efficiency of the split NAT protein in fusions and thus the biosensor's readout. The split antibiotic resistance markers appear to act as more neutral fusion partners than some others, for example fluorescent proteins whose fusion can affect the folding or stability of the insertion partner. This is perhaps in part because we previously devoted considerable effort in the selection of fusion partners and insertion sites within these antibiotic resistance genes that gave a good linear relationship between

the thermodynamic stability of the inserted protein and the antibiotic resistance readout.[25] Also, at least in part due to these reasons, the direct antibiotic resistance readouts of these APH- and NAT-based fusions appear to provide a more sensitive assessment for *in vivo* protein stability than analysis of protein levels by immunoblotting.

Because the tripartite fusion design can link protein stability to antibiotic resistance for unrelated antibiotic resistance genes (APH and NAT), it may allow two independent readouts of protein stability within a single cell. In summary, the results demonstrate that the tripartite fusion system provides a convenient tool that is sensitive to *in vivo* protein stability in the cytosol of *S. cerevisiae*.

Ligand Binding Enhances Stability Readout. Ligand binding thermodynamically stabilizes the binding partner in a way that is related to the binding affinity and the concentrations of the two binding partners.[33] To explore whether ligand binding-induced stabilization could be detected using our tripartite system in yeast, we expressed the APH-Im7 WT tripartite fusion together with Im7's natural binding partner protein, colicin E7, as a nuclease deficient variant fragment (residues 63−193, variant H162A).[34] Indeed, coexpression of the colicin E7 H162A fragment caused a significant increase in antibiotic resistance and a minor increase in APH-Im7 WT protein levels relative to coexpression of an empty vector control (Figure 3, Supplementary Figure 4), indicating that the cytosolic tripartite fusion system may allow detection of changes in *in vivo* stability resulting from intermolecular interactions

Tripartite Biosensors Allow Study of Neuropathological Proteins and Prion Proteins. We wondered if alterations in protein solubility could also impact the antibiotic resistance readout of our tripartite fusions. If true, these fusions might be useful in the *in vivo* study of pathologically misfolded or aggregation-prone proteins. We therefore assessed the pheno-
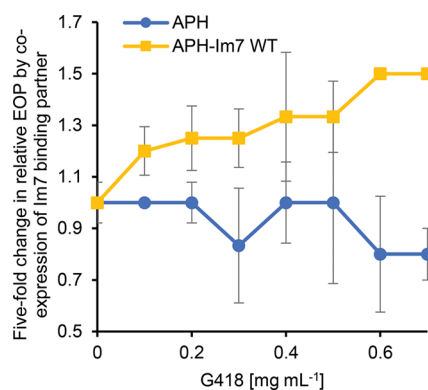

Figure 3. Expression of an Im7 binding partner together with the APH-Im7 WT tripartite fusion increases antibiotic resistance. The plot shows the 5-fold change in the efficiency of plating (EOP) of *S. cerevisiae* strains expressing either only the APH WT (strain VES271) or the APH-Im7 WT (strain VES274) tripartite fusion together with Im7's binding partner protein, the nuclease fragment of colicin E7 (residues 63−193) relative to the efficiency of plating of cells expressing the APH WT (strain VES270), or APH-Im7 WT (strain VES273) tripartite fusion with an empty vector. The colicin E7 variant H162A was used to reduce the otherwise lethal nuclease activity of this colicin.[34] Serial dilution spotting assays were used to score cell growth on synthetic complete (SC) agar lacking uracil and tryptophan, supplemented with 2% galactose and 2% raffinose, and supplemented with increasing concentrations of the antibiotic G418. The experiment was performed in quadruplicate, and error bars indicate ±1 SD.

typic readout of tripartite sensors fused with bonafide representatives of pathological protein misfolding. We used the disease-relevant Aβ42 peptide and α-synuclein protein, and the prion forming proteins Rnq1 and Sup35.[4,35]

Aβ42. Misfolding of the peptide Aβ42 is closely associated with Alzheimer's disease.[36] Humanized yeast models for Aβ42 involve different misfolded or aggregation states of this peptide, which, to some extent, depend on the reporter system used. Cytotoxic overexpression approaches involving the fusion of Aβ42 with GFP or with enzymes that can be linked to growth such as dihydrofolate reductase can, at least superficially, mimic different oligomerization and aggregation states of Aβ42.[10,13,14,17,18]

To provide a complementary yeast model that relies on a different reporter principle than these previously developed approaches, we inserted Aβ42 into our APH and NAT tripartite biosensors (Figure 4a and Supplementary Figure 5a).

Cells expressing tripartite fusions with Aβ42 insertions showed substantially lower titers on antibiotic containing plates than cells expressing the same markers but with only a GS linker inserted at the same position (Figure 4b, c and Supplementary Figures 5b, 6a−c, 7). Cells expressing an aggregation deficient, less hydrophobic Aβ42 variant, Aβ42 F19T F20T I31P, showed higher levels of antibiotic resistance, similar to those shown by the GS linker-alone controls (Figure 4b, c and Supplementary Figures 5b and 7). To test if only the hydrophobic character of the WT Aβ42 peptide fused between the marker halves was the denominator for the observed antibiotic resistance phenotype, we generated tripartite fusions with the shorter Aβ variant, Aβ40, and with an Aβ42 variant with a scrambled amino acid sequence which, if true, should show similar resistance phenotypes.[37] For cells expressing tripartite fusions with Aβ40 we observed up to ~5-fold higher and with the scrambled Aβ42 variant up to ~10-fold higher antibiotic resistance readouts (Supplementary Figures 6c and 7) compared to cells expressing tripartite fusions with wild-type Aβ42 (Supplementary Figure 6c and 7). These observations suggested Aβ42's sequence characteristic as determinant for the conferred antibiotic resistance phenotype. In the absence of antibiotic, cell titers of tripartite fusion expressing strains were all very similar, indicating that no Aβ42- or Aβ40-induced cytotoxicity was observed. Except for Sup35 full length (see below), no toxicity was observed for any of the tripartite fusions described in this work. The lack of toxicity is likely due to the moderate expression level of the tripartite fusions by driving it from the *GAL1* promoter from a single chromosomal gene copy. The low/moderate tripartite protein level makes our results more physiologically relevant than massive overexpression commonly used historically, expression levels that often lead to toxicity.[6,11,38] Expression levels of the mRNA for the Aβ42 tripartite fusions and the constructs described below were all comparable (Supplementary Figure 8), which led us to conclude that transcription or mRNA stability did not explain the differential resistance readouts observed. Chase experiments and immunohistochemical detection of the Aβ42 and linker tripartite fusions indicated enhanced proteolytic susceptibility of WT Aβ42 compared to Aβ42 F19T F20T I31P and GS linker-only fusions (Figure 4e−g and Supplementary Figure 5c), which may explain the differential antibiotic resistance phenotype. This degradation was inhibited by proteasome inhibitors (Figure 4f and Supplementary Figure 5c). Our results are consistent with previous observations that proteasomal degradation is involved in the clearance of unstable Aβ42.[39] When present in low
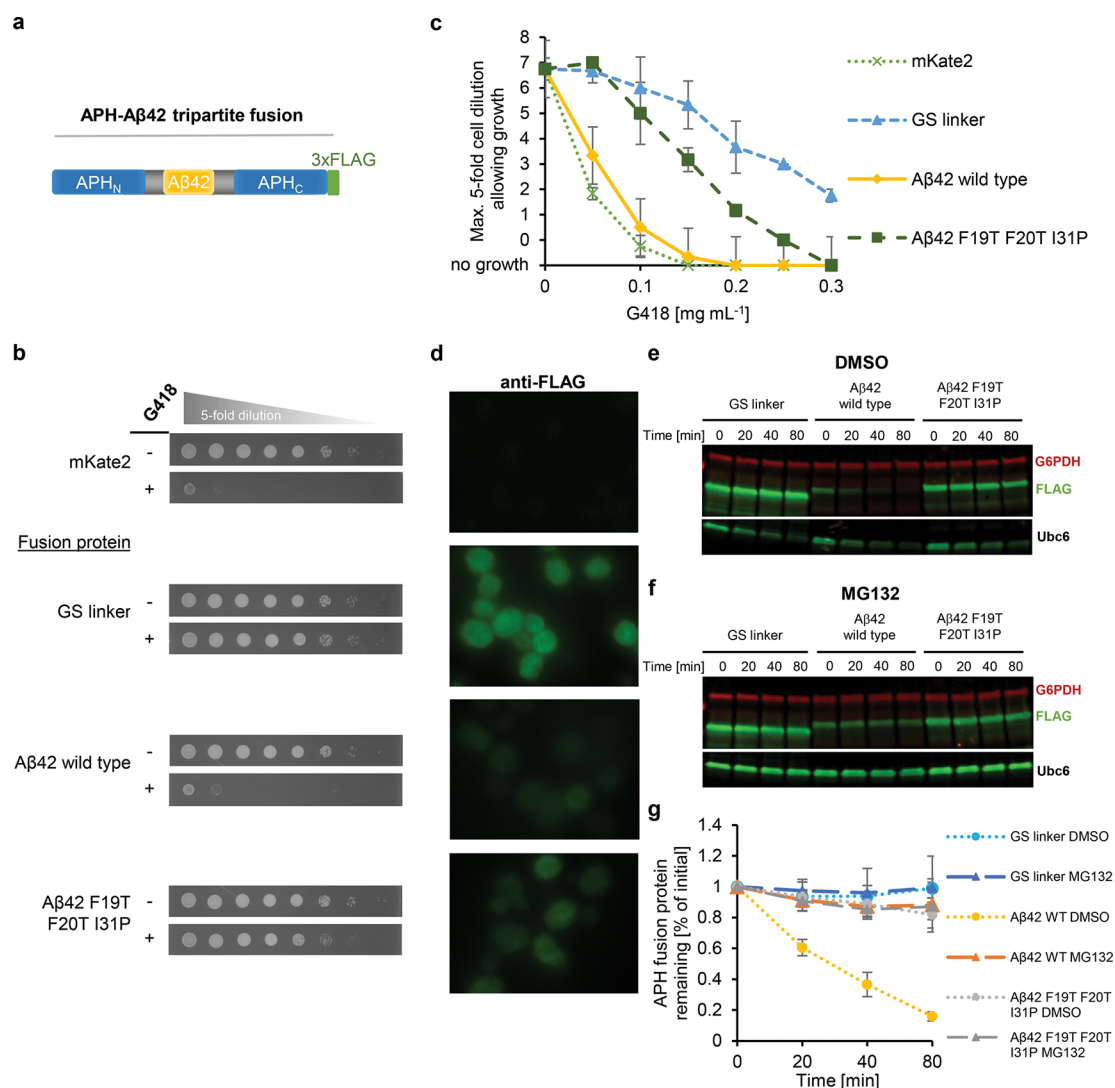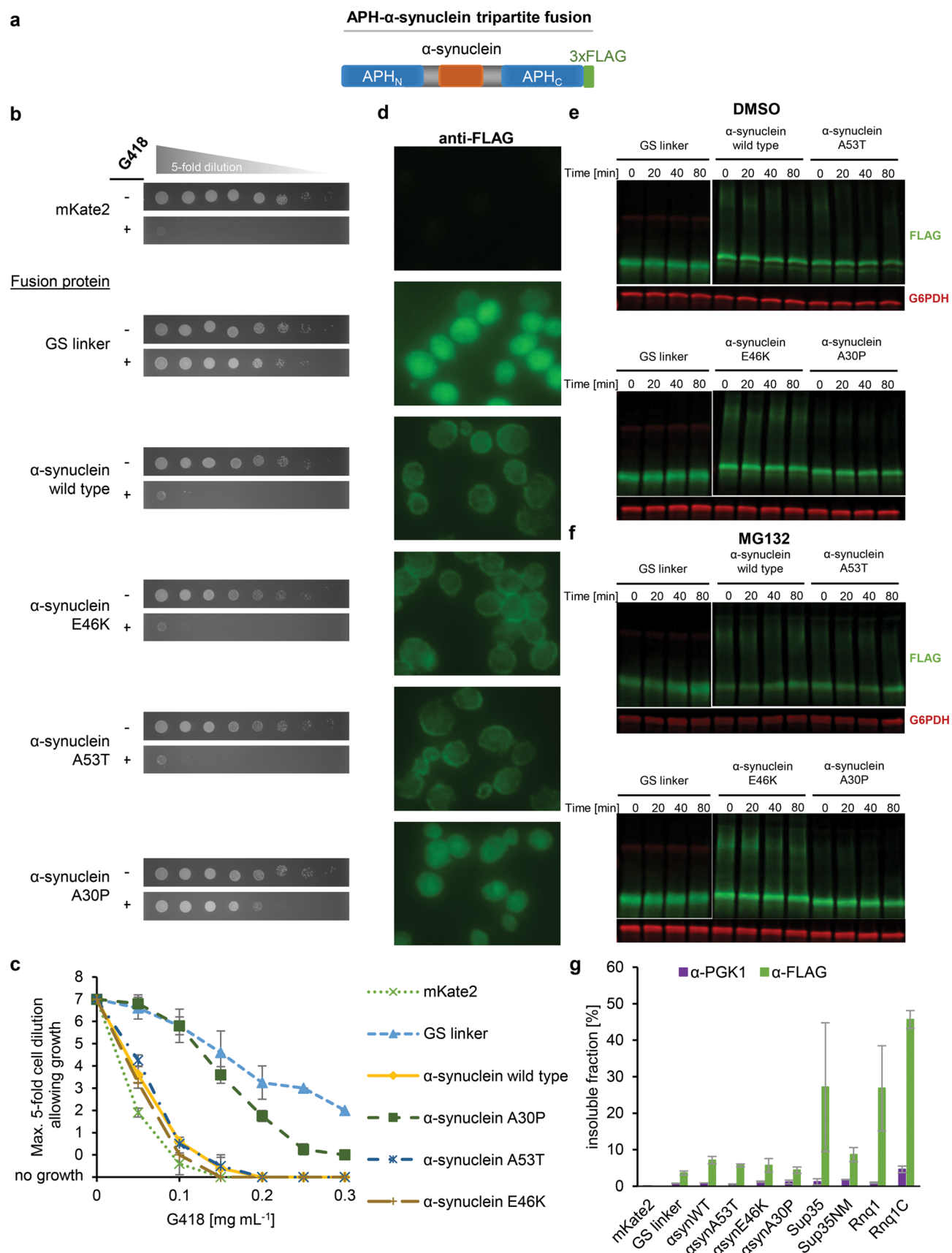
Figure 4. Antibiotic resistance conferred by the APH-Aβ42 tripartite biosensor varies depending on the *in vitro* stability of the Aβ42 insert. (a) Schematic diagram of the APH-Aβ42 tripartite fusion. Cells were grown to early or mid log phase in SC media supplemented with 2% raffinose and 0.1% glucose prior to induction of the tripartite fusions. (b) Antibiotic resistance of yeast cells expressing either a non-G418 resistant control protein, mKate2 (VES650), or various G418 resistant APH constructs containing just a GS linker insert (VES657), or the additional insertion of WT Aβ42 (VES702) or the aggregation deficient Aβ42 variant, Aβ42 F19T F20T I31P (VES700). Fivefold serial dilution spotting assays were used to score cell growth on SC agar media supplemented without or with 0.1 mg mL^{-1} G418 (indicated by a − or +, respectively, in the G418 column). (c) Quantification of the antibiotic resistance phenotypes of the Aβ42 tripartite fusions over the range of 0−0.3 mg mL^{-1} G418 as observed in spotting assays. The data plotted are from four experiments; error bars indicate ±1 SD. (d) Immunohistochemical detection using anti-FLAG antibodies to determine the cellular localization of the APH-Aβ42 tripartite fusions. Prior to the detection, expression of tripartite fusions was induced for 4 h with 2% galactose. Strain order from top to bottom was the same as in (b). Exposure time was 50 ms. (e and f) To assess the stability of the APH-Aβ42 fusions, cycloheximide chase experiments were performed for the indicated times followed by immunoblotting against the FLAG epitope on the C terminus of the fusions against G6PDH as a loading control and against the proteasome substrate Ubc6 as to get an indication of the efficiency of proteasome inhibition. Prior to the chase experiments, tripartite expression was induced for 6 h with 2% galactose, and cells were treated with either dimethyl sulfoxide (DMSO) as control (e) or the proteasome inhibitor MG132 dissolved in DMSO (f). Cycloheximide chase experiments of cells expressing APH constructs containing just a GS linker insert (yXD622, or the additional insertion of WT Aβ42 (yXD623) or Aβ42 F19T F20T I31P (yXD624) were performed in pdr5Δ strain backgrounds. (g) Quantification of APH fusion levels relative to their initial cellular amounts in cycloheximide chase assays. These experiments were performed in triplicate; error bars indicate ±1 SD.

concentrations, soluble Aβ42 has been found to be efficiently cleared by the quality control machinery, especially the ubiquitin proteasome system, whose reduced function has been implicated in Alzheimer's disease.[40] Increased steady state levels of Aβ42 are known to enhance primary nucleation events, a prerequisite for Aβ42-associated disease states.[41] Understanding and enhancing the degradation of the Aβ peptide has been suggested as a strategy for targeting Alzheimer's disease.[39] As our phenotypic readout for WT Aβ42 tripartite fusions involves

proteolytic processing of Aβ42, our method may be useful in further exploring the stability of intracellular Aβ42. For example, our approach could help determine which factors contribute to the stability or clearance of unstable Aβ42 conformers and thus give further insight into the role of Aβ42 in Alzheimer's disease.

α-Synuclein. We also explored the utility of the tripartite fusion system in assessing the folding state of α-synuclein, a protein involved in the second most prevalent neuropathogenic disorder, Parkinson's disease.[42] This disease has been closely

Figure 5. Antibiotic resistance conferred by the APH-α-synuclein tripartite biosensors varies depending on the ability of the α-synuclein inserts to interact with the membrane. (a) Schematic diagram of the APH-α-synuclein tripartite fusion. Cells were grown to early or mid log phase in SC media supplemented with 2% raffinose and 0.1% glucose prior to induction of the tripartite fusions. (b) Antibiotic resistance of yeast cells expressing either a non-G418 resistant control protein, mKate2 (VES650), or various G418 resistant APH constructs containing just a GS linker insert (VES657) or the

Figure 5. continued

additional insertion of: WT α-synuclein (VES683), α-synuclein E46K (VES687), α-synuclein A53T (VES685), or α-synuclein A30P (VES706). Fivefold serial dilution spotting assays were used to score cell growth on SC agar media supplemented without or with 0.15 mg mL^{-1} G418 (indicated by a − or +, respectively, in the G418 column). (c) Quantification of antibiotic resistance phenotypes of the α-synuclein tripartite fusions over the range of 0−0.3 mg mL^{-1} G418 as obtained from spotting assays. The reported data are from five experiments; error bars indicate ±1 SD. (d) Immunohistochemical detection using anti-FLAG antibodies to determine the cellular localization of the APH-α-synuclein fusions. Prior to the detection, expression of tripartite fusions was induced for 8 h with 2% galactose. Strain order from top to bottom was the same as in (b). Exposure time 50 ms. (e and f) To assess the stability of the APH-α-synuclein fusions, cycloheximide chase experiments were performed for the indicated times followed by immunoblotting against the FLAG epitope on the C terminus of the fusions and against G6PDH as loading control. Prior to the chase experiments, tripartite expression was induced for 6 h with 2% galactose, and cells were treated with either DMSO (e) or the proteasome inhibitor MG132 (f). (g) Lysates of yeast cells that had been expressing APH fusions for 12 h were separated into soluble and insoluble protein fractions to determine the aggregation propensities for APH fusions containing α-synuclein (α-syn) WT and variants A53T, E46K, and A30P (yeast strains VES683, VES685, VES687, and VES706, respectively), Sup35 (strain yHH86), Sup35NM (yHH88), Rnq1 (yHH90), Rnq1C (yHH93), or just the GS linker (VES657). The relative amount of insoluble APH tripartite fusion relative to the total amount of APH tripartite protein in the cell lysates was determined by quantitative Western blotting using antibodies against the FLAG epitope at the C terminus of the fusions (α-FLAG) and against phosphoglycerate kinase (α-PGK1) for normalization. Cells expressing only the fluorescent protein mKate2 (VES650) were used as a control. The experiment was performed in triplicate, and error bars indicate ±1 SD.

linked to missense mutations in and multiplication of the α-synuclein gene.[42] To assess the folding of α-synuclein in yeast using the tripartite system, we fused the split APH marker with cDNA from WT α-synuclein and the disease-associated α-synuclein mutants A53T, E46K, and A30P (Figure 5a).

Others have found that the A53T and E46K mutants exhibit an accelerated aggregation rate compared to that of WT α-synuclein.[43,44] Less consensus exists concerning the effect of the A30P mutation; there are reports that this variant fibrillizes more slowly,[43,45] more rapidly,[46,47] and at a similar rates compared to other α-synuclein variants *in vitro*.[48] In our tripartite system, yeast cells expressing APH tripartite fusions with α-synuclein A30P showed strikingly higher antibiotic resistance than fusions with WT α-synuclein or the A53T and E46K variants (Figure 5b, c Supplementary Figure 6d). In contrast to our WT Aβ42 fusion, tripartite fusions with WT α-synuclein and its variants were proteolytically stable (Figure 5e, f). However, the intracellular detection patterns of the α-synuclein fusions varied in a way that correlated with their antibiotic resistance behavior: fusions with WT α-synuclein, A53T, or E46K were primarily detected at the cell membrane, whereas α-synuclein A30P fusions were mostly dispersed throughout the cytosol (Figure 5d). These findings are in keeping with previously published yeast models of α-synuclein biology.[11,49] Our observation that the α-synuclein A30P fusion was not found primarily at the cell membrane may be explained by α-synuclein A30P's low membrane binding capacity *in vitro*.[50] We also found SDS stable oligomeric species for the WT α-synuclein, E46K, and A53T fusions as indicated by Western blotting (Figure 5e). Although detectable, these high molecular weight species do not appear to be present in high concentrations, as lysate fractionation assays and SDD-AGE showed high solubility for all tripartite α-synuclein variants (Figure 5g, Supplementary Figure 9a). However, their presence is consistent with their phenotypic readout and differential localization patterns as compared to fusions with A30P. Labile oligomers of α-synuclein fusions have been observed.[51] It has been suggested that the early stages of α-synuclein aggregation consist of disordered oligomeric species and accumulation of monomeric α-synuclein within lipid-like droplets, which may serve as precursors to amyloids.[51,52] It is therefore possible that WT α-synuclein, A53T, and E46K tripartite fusions, which display decreased antibiotic resistance readouts, may be localized at the membrane and be mimicking the misfolding events that are associated with lipid binding. Thus, our APH-α-synuclein folding biosensors could possibly be used to screen for

small molecules and cellular components that modify α-synuclein stability or association.

α-Synuclein variant fusions with the NAT biosensor did not yield any differential phenotypic readout on nourseothricin containing agar plates in comparison to GS linker-only fusions. This was also the case for NAT fusions containing other aggregation-prone proteins such as Rnq1 and Sup35, which are described below. As discussed earlier, the NAT tripartite context, but conceivably also the APH fusion context, may in some cases increase its aggregation propensity by changing its overall solubility, interfere with the protein's folding, or sterically affect the formation of the amyloid structure, which has also been observed with other chimera-based approaches.[15,17] As a result, the NAT construct may not provide as useful of an antibiotic resistance readout as the APH reporter depending on the specific test protein used.

Rnq1 and Sup35. Prions are misfolded proteins that can transmit their misfolded shape onto normally folded molecules of the same protein and propagate this misfolded status from cell to cell. Although commonly associated with mammalian diseases such as mad cow disease, prion proteins are not exclusive to mammals and other animals, but occur in many other kingdoms, including yeast.[35,53] In yeast, prion formation occurs stochastically and is thought to represent a protein encoded, epigenetic phenotypic switch.[35,53] Studies on yeast prion formation have extended our understanding of prion aggregation, inheritance, and prion encoded memory effects, and have allowed the identification of trans acting proteins and exogenous factors that affect prion formation.[53] Generally, aggregation of yeast prion proteins is dependent on the presence of preexisting prion structures in the cell and is mediated by the protein's prion domain (PrD).[54] These PrDs are generally intrinsically disordered Gln (Q)- and/or Asn (N)-rich sequence stretches.[54] Archetypal representatives of yeast prion proteins are the translation terminator Sup35, which aggregates to form the prion [PSI$^+$], and the Rnq1 protein, whose function has not yet been elucidated but clearly aggregates to form the prion [PIN$^+$] which is also known as prion [RNQ$^+$].[55] Fluorescent reporter proteins have been used in a variety of innovative approaches to assess prion formation behavior in yeast.[22,23]

To test if our tripartite fusion system can be used to assess prion aggregation propensity, we inserted Rnq1 and Sup35 into our APH tripartite system (Figure 6a). For Rnq1, we fused the complete protein encoding sequence as well as its prion forming domain (Rnq1C), which spans the protein's Q/N-rich C-
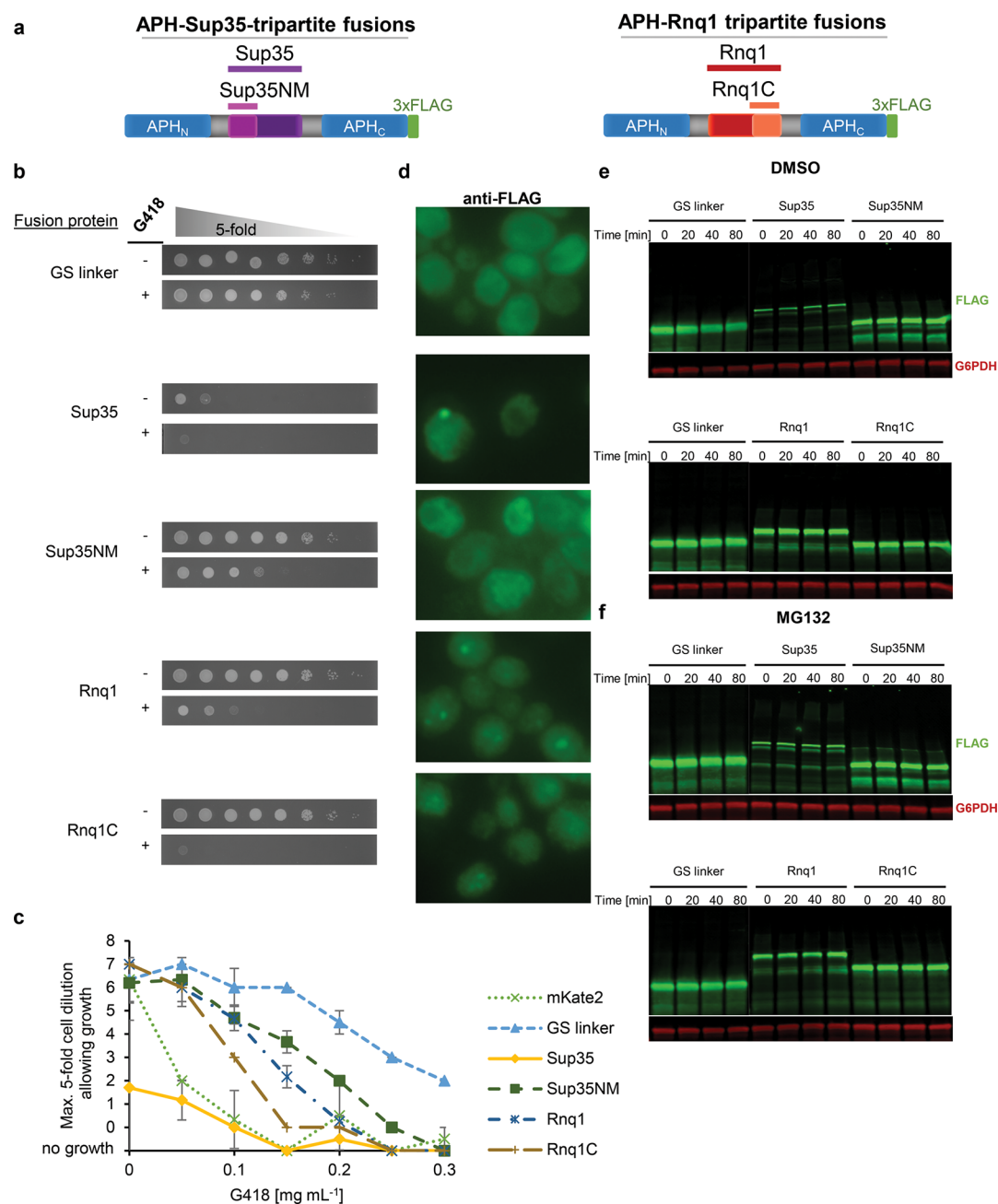
Figure 6. Antibiotic resistance of APH tripartite biosensors fused with yeast prion proteins depends on the aggregation propensities of the insets. (a) Schematic diagram of the APH-Sup35 and APH-Rnq1 tripartite fusions. The complete Sup35 protein sequence or just its N-terminal prion domain (Sup35NM) was inserted into the APH protein. For the APH-Rnq1 tripartite fusions, the complete Rnq1 sequence or its C-terminal prion domain (Rnq1C) was inserted. Yeast cells were grown to early or mid log phase in SC media supplemented with 2% raffinose and 0.1% glucose prior to induction of the tripartite fusions. (b) Antibiotic resistance of cells expressing various G418 resistant APH constructs containing just a GS linker (VES657) or the additional insertion of the full length Sup35 sequence (yHH86), Sup35NM (yHH88), full length Rnq1 (yHH90), or Rnq1C (yHH93). Fivefold serial dilution spotting assays were used to score cell growth on SC agar media supplemented without or with 0.15 mg mL^{-1} G418 (indicated by a − or +, respectively, in the G418 column). (c) Quantification of antibiotic resistance phenotypes of the Sup35 and Rnq1 tripartite fusions over the range of 0−0.3 mg mL^{-1} G418 observed in spotting assays. Plotted are the data from five experiments; error bars indicate ±1 SD. (d) Immunohistochemical detection using anti-FLAG antibodies to determine the cellular localization of the APH−prion fusions. Prior to the detection, expression of tripartite fusions was induced for 8 h with 2% galactose. Strain order from top to bottom was the same as in (b). Exposure time was 100 ms. (e and f) To assess the stability of the APH−prion fusions, cycloheximide chase experiments were performed for the indicated times followed by immunoblotting against the FLAG epitope on the C terminus of the fusions and against G6PDH as a loading control. Prior to the chase experiments, expression of the tripartite fusions was induced for 6 h, and cells were treated with either DMSO (e) or the proteasome inhibitor MG132 (f).

terminal half (residues 153−405).[56] Similarly for Sup35, the complete Sup35 sequence as well as its Sup35NM domain, which comprises a prion forming region (N, residues 1−123) and the highly charged prion stabilizing middle domain (M,

residues 124−253),[57] were inserted into the APH tripartite construct.

Cells expressing fusions with full length Rnq1 and especially Rnq1C showed substantially lower titers on antibiotic

containing plates than did constructs containing only GS linker insertions (Figure 6b, c and Supplementary Figure 6e). Consistent with the antibiotic resistance readout, results obtained suggested that Rnq1 tripartite fusions form proteolytically stable aggregates with amyloid-like structures (Supplementary Figure 9a). Collectively, these findings indicate the formation of prion particles or aggregates of the Rnq1 tripartite fusions *in vivo*, which is consistent with previous studies and presumably leads to the observed antibiotic sensitivity.[57] Importantly, we did not obtain any evidence for the preexistence of endogenous [PSI⁺] or [PIN⁺] structures in our strains (Supplementary Figures 9b, 10), structures that could possibly have affected the aggregation propensity of the prion protein tripartite fusions.[22,23,57−59]

Cells expressing fusions with prion proteins full length Sup35 and to a much lesser extent the Sup35NM domain also exhibited decreased titers on antibiotic containing plates relative to strains expressing the GS linker-only control (Figure 6b, c and Supplementary Figure 6e). Consistent with the antibiotic resistance phenotypes, Sup35 full length and to a lesser extent Sup35NM tripartite fusion were found to aggregate (Figure 5g, 6e, f) and detected in visible puncta in the cell (Figure 6d). Results of SDD-AGE experiments showed that the Sup35NM but not Sup35 full length tripartite fusions formed SDS-insoluble polymers (Supplementary Figure 9a). The results suggested a greater aggregation propensity for fusions with Sup35 full length as compared to Sup35NM. However, the observation was confounded by the fact that transient overexpression of the Sup35 full length but not Sup35NM tripartite was cytotoxic, as apparent from lower cell growth even in the absence of antibiotic (Figure 6b, c, Supplementary Figure 11). Although we could not detect any [PSI⁺] prion structures (Supplementary Figure 9a), this toxicity has previously been attributed to the sequestration of endogenous Sup35 into aggregates.[52,56] The presence of [PIN⁺], which we did not find evidence for in any of our strains (Supplementary Figures 9b and 10), would be required to enhance [PSI⁺] formation through excess levels of Sup35 full length or the Sup35NM domain.[58] Coexpression of Sup35's essential C-terminal domain with the Sup35 full length tripartite fusion could alleviate cytotoxicity as has been previously seen (Supplementary Figure 11).[56,60] Although cytotoxicity can interfere with the antibiotic readout of our tripartite fusion system, such cytotoxicity is fortunately immediately evident from control spot titers plated in the absence of antibiotic. The tripartite system with Sup35NM fusions may in the future be useful to explore factors that modulate the solubility of the prion domain *in vivo*.

SUMMARY AND CONCLUSIONS

Changes in protein stability or solubility play a key role in many fundamental cellular events and are involved in misfolding processes that have been linked to a wide variety of human diseases. In this work, we present yeast biosensors that work to help determine the *in vivo* protein stability or aggregation propensity of specific proteins linked to protein misfolding diseases. Our goal was to develop a versatile biosensor in yeast that allows a quantitative readout for protein stability and aggregation propensity. The system we developed features a tripartite design that couples protein folding or solubility to antibiotic resistance. This key advantage should make it possible to design high-throughput screens and selections for host factors that affect protein stability or solubility. In addition, the APH and NAT marker genes are functional in cells of other species, in

the case of NAT, >100 different species,[61] making this tripartite fusion approach potentially widely transferrable to other organisms. Importantly, our biosensor approach does not involve any cellular toxicity, which is another main advantage of the system. Applying this tripartite fusion approach to prion proteins Sup35 and Rnq1 allowed us to determine their aggregation propensities based on antibiotic resistance readouts. For Aβ42 and α-synuclein fusions, antibiotic resistance appears to depend on other disease-related properties such as proteolytic sensitivity and the tendency to localize at membranes. Because biosensors are based on different underlying principles, each has their advantages and limitations. Like other chimera-based biosensors, our tripartite approach might modulate the solubility of the test protein and does require additional validation, including follow-up *in vitro* characterization of the conferred phenotype. Both antibiotic resistance markers determinate function in the cytosol, limiting our approach to proteins that can be expressed in this compartment. Despite these inherent limitations, we feel our biosensors are a valuable tool for detecting protein stability and aggregation states in living cells. As demonstrated in our study, the tripartite approach appears to provide a convenient and powerful experimental platform that could be used to screen for protein variants, host factors, or small molecules that modulate the disease-related properties of amyloid or prion-prone proteins *in vivo*.

METHODS

Detailed descriptions of all methods are provided in the Supporting Information.

ASSOCIATED CONTENT

SI **Supporting Information**

The Supporting Information is available free of charge at https://pubs.acs.org/doi/10.1021/acschembio.0c00083.

> Supporting figures and tables and detailed descriptions of all experimental procedures, comprising the construction of the tripartite fusions, optimization of the biosensors, spotting assays and MIC determination, the tripartite Im7 fusion solubility assay, analysis of the aggregation propensities of tripartite fusions, quantitative Western blotting, cycloheximide chase assay to determine proteolytic stability of tripartite fusions, immunohistochemical detection of the cellular localization of tripartite fusions, SDD-AGE to detect SDS-insoluble amyloid structures, quantitative reverse transcription PCR to determine expression levels of the tripartite fusions, and treatment with guanidine hydrochloride to cure cells from preexisting prions (PDF)

AUTHOR INFORMATION

Corresponding Author

James C.A. Bardwell − *Department of Molecular, Cellular, and Developmental Biology and Howard Hughes Medical Institute, University of Michigan, Ann Arbor, Michigan 48109-1085, United States;* ⊙ orcid.org/0000-0003-1683-1944; Phone: 734-764-8028; Email: jbardwel@umich.edu

Authors

Veronika Sachsenhauser − *Department of Molecular, Cellular, and Developmental Biology and Howard Hughes Medical Institute, University of Michigan, Ann Arbor, Michigan 48109-1085, United States; Department of Chemistry, Technical University Munich, 85748 Garching, Germany*

Xiexiong Deng — *Department of Molecular, Cellular, and Developmental Biology and Howard Hughes Medical Institute, University of Michigan, Ann Arbor, Michigan 48109-1085, United States*

Hyun-hee Kim — *Department of Molecular, Cellular, and Developmental Biology and Howard Hughes Medical Institute, University of Michigan, Ann Arbor, Michigan 48109-1085, United States*

Maja Jankovic — *Department of Molecular, Cellular, and Developmental Biology and Howard Hughes Medical Institute, University of Michigan, Ann Arbor, Michigan 48109-1085, United States*

Complete contact information is available at:
https://pubs.acs.org/10.1021/acschembio.0c00083

Author Contributions

Notes

ACKNOWLEDGMENTS

REFERENCES

(1) Aguzzi, A., and Lakkaraju, A. K. K. (2016) Cell biology of prions and prionoids: a status report. *Trends Cell Biol. 26*, 40−51.

(2) Banani, S. F., Lee, H. O., Hyman, A. A., and Rosen, M. K. (2017) Biomolecular condensates: Organizers of cellular biochemistry. *Nat. Rev. Mol. Cell Biol. 18*, 285−298.

(3) Tyedmers, J., Mogk, A., and Bukau, B. (2010) Cellular strategies for controlling protein aggregation. *Nat. Rev. Mol. Cell Biol. 11*, 777−788.

(4) Khurana, V., and Lindquist, S. (2010) Modelling neurodegeneration in Saccharomyces cerevisiae: Why cook with baker's yeast? *Nat. Rev. Neurosci. 11*, 436−449.

(5) Park, S.-K. S. K., Pegan, S. D., Mesecar, A. D., Jungbauer, L. M., LaDu, M. J. J., and Liebman, S. W. (2011) Development and validation of a yeast high-throughput screen for inhibitors of A 42 oligomerization. *Dis. Models & Mech. 4*, 822−831.

(6) Treusch, S., Hamamichi, S., Goodman, J. L., Matlack, K. E. S. S., Chung, C. Y., Baru, V., Shulman, J. M., Parrado, A., Bevis, B. J., Valastyan, J. S., Han, H., Lindhagen-Persson, M., Reiman, E. M., Evans, D. A., Bennett, D. A., Olofsson, A., DeJager, P. L., Tanzi, R. E., Caldwell, K. A., Caldwell, G. A., and Lindquist, S. (2011) Functional links between Aβ toxicity, endocytic trafficking, and Alzheimer's disease risk factors in yeast. *Science 334*, 1241−1245.

(7) Matlack, K. E. S., Tardiff, D. F., Narayan, P., Hamamichi, S., Caldwell, K. A., Caldwell, G. A., and Lindquist, S. (2014) Clioquinol promotes the degradation of metal-dependent amyloid-ß (Aß) oligomers to restore endocytosis and ameliorate Aß toxicity. *Proc. Natl. Acad. Sci. U. S. A. 111*, 4013−4018.

(8) Waldo, G. S., Standish, B. M., Berendzen, J., and Terwilliger, T. C. (1999) Rapid protein-folding assay using green fluorescent protein. *Nat. Biotechnol. 17*, 691−695.

(9) Cabantous, S., Terwilliger, T. C., and Waldo, G. S. (2005) Protein tagging and detection with engineered self-assembling fragments of green fluorescent protein. *Nat. Biotechnol. 23*, 102−107.

(10) Caine, J., Sankovich, S., Antony, H., Waddington, L., Macreadie, P., Varghese, J., and Macreadie, I. (2007) Alzheimer's Aβ fused to green fluorescent protein induces growth stress and a heat shock response. *FEMS Yeast Res. 7*, 1230−1236.

(11) Outeiro, T. F., and Lindquist, S. (2003) Yeast cells provide insight into alpha-synuclein biology and pathobiology. *Science 302*, 1772−1775.

(12) Lázaro, D. F., Rodrigues, E. F., Langohr, R., Shahpasandzadeh, H., Ribeiro, T., Guerreiro, P., Gerhardt, E., Kröhnert, K., Klucken, J., Pereira, M. D., Popova, B., Kruse, N., Mollenhauer, B., Rizzoli, S. O., Braus, G. H., Danzer, K. M., and Outeiro, T. F. (2014) Systematic comparison of the effects of alpha-synuclein mutations on its oligomerization and aggregation. *PLoS Genet. 10*, No. e1004741.

(13) Nair, S., Traini, M., Dawes, I. W., and Perrone, G. G. (2014) Genome-wide analysis of Saccharomyces cerevisiae identifies cellular processes affecting intracellular aggregation of Alzheimer's amyloid-β42: Importance of lipid homeostasis. *Mol. Biol. Cell 25*, 2235−2249.

(14) D'Angelo, F., Vignaud, H., Di Martino, J., Salin, B., Devin, A., Cullin, C., and Marchal, C. (2013) A yeast model for amyloid-aggregation exemplifies the role of membrane trafficking and PICALM in cytotoxicity. *Dis. Models & Mech. 6*, 206−216.

(15) Cabantous, S., Rogers, Y., Terwilliger, T. C., and Waldo, G. S. (2008) New molecular reporters for rapid protein folding assays. *PLoS One 3*, No. e2387.

(16) Hamada, D., Tsumoto, K., Sawara, M., Tanaka, N., Nakahira, K., Shiraki, K., and Yanagihara, I. (2008) Effect of an amyloidogenic sequence attached to yellow fluorescent protein. *Proteins: Struct., Funct., Genet. 72*, 811−821.

(17) Bagriantsev, S., and Liebman, S. (2006) Modulation of Aβ42 low-n oligomerization using a novel yeast reporter system. *BMC Biol. 4*, 1−12.

(18) Morell, M., de Groot, N. S., Vendrell, J., Avilés, F. X., and Ventura, S. (2011) Linking amyloid protein aggregation and yeast survival. *Mol. BioSyst. 7*, 1121−1128.

(19) França, M. B., Lima, K. C., and Eleutherio, E. C. A. (2017) Oxidative stress and amyloid toxicity: insights from yeast. *J. Cell. Biochem. 118*, 1442−1452.

(20) Braun, R. J. (2012) Mitochondrion-mediated cell death: dissecting yeast apoptosis for a better understanding of neurodegeneration. *Front. Oncol. 2*, 1−14.

(21) Schneider, K. L., Nyström, T., and Widlund, P. O. (2018) Studying spatial protein quality control, proteopathies, and aging using different model misfolding proteins in S. cerevisiae. *Front. Mol. Neurosci. 11*, 1−13.

(22) Khan, T., Kandola, T. S., Wu, J., Venkatesan, S., Ketter, E., Lange, J. J., Rodriguez Gama, A., Box, A., Unruh, J. R., Cook, M., and Halfmann, R. (2018) Quantifying nucleation in vivo reveals the physical basis of prion-like phase behavior. *Mol. Cell 71*, 155−168.

(23) Newby, G. A., Kiriakov, S., Hallacli, E., Kayatekin, C., Tsvetkov, P., Mancuso, C. P., Bonner, J. M., Hesse, W. R., Chakrabortee, S., Manogaran, A. L., Liebman, S. W., Lindquist, S., and Khalil, A. S. (2017) A genetic tool to track protein aggregates and control prion inheritance. *Cell 171*, 966−979.

(24) Foit, L., Morgan, G. J., Kern, M. J., Steimer, L. R., von Hacht, A. A., Titchmarsh, J., Warriner, S. L., Radford, S. E., and Bardwell, J. C. A. (2009) Optimizing protein stability and folding in vivo. *Mol. Cell 36*, 861−871.

(25) Malik, A., Mueller-Schickert, A., and Bardwell, J. C. A. (2014) Cytosolic selection systems to study protein stability. *J. Bacteriol. 196*, 4333−4343.

(26) Van Rosmalen, M., Krom, M., and Merkx, M. (2017) Tuning the Flexibility of Glycine-Serine Linkers to Allow Rational Design of Multidomain Proteins. *Biochemistry 56*, 6565−6574.

(27) Erickson, H. P. (2009) Size and shape of protein molecules at the nanometer level determined by sedimentation, gel filtration, and electron microscopy. *Biol. Proced. Online 11*, 32−51.

(28) Capaldi, A. P., Kleanthous, C., and Radford, S. E. (2002) Im7 folding mechanism: Misfolding on a path to the native state. *Nat. Struct. Biol. 9*, 209−216.

(29) Spence, G. R., Capaldi, A. P., and Radford, S. E. (2004) Trapping the on-pathway folding intermediate of Im7 at equilibrium. *J. Mol. Biol. 341*, 215−226.

(30) Pashley, C. L., Morgan, G. J., Kalverda, A. P., Thompson, G. S., Kleanthous, C., and Radford, S. E. (2012) Conformational Properties of the Unfolded State of Im7 in Nondenaturing Conditions. *J. Mol. Biol. 416*, 300−318.

(31) Ghaemmaghami, S., and Oas, T. G. (2001) Quantitative protein stability measurement in vivo. *Nat. Struct. Biol. 8*, 879−882.

(32) Ignatova, Z., and Gierasch, L. M. (2004) Monitoring protein stability and aggregation in vivo by real-time fluorescent labeling. *Proc. Natl. Acad. Sci. U. S. A. 101*, 523−528.

(33) Du, X., Li, Y., Xia, Y. L., Ai, S. M., Liang, J., Sang, P., Ji, X. L., and Liu, S. Q. (2016) Insights into protein−ligand interactions: Mechanisms, models, and methods. *Int. J. Mol. Sci. 17*, 1−34.

(34) Huang, H., and Yuan, H. S. (2007) The conserved asparagine in the HNH motif serves an important structural role in metal finger endonucleases. *J. Mol. Biol. 368*, 812−821.

(35) Jarosz, D. F., and Khurana, V. (2017) Specification of physiologic and disease states by distinct proteins and protein conformations. *Cell 171*, 1001−1014.

(36) Selkoe, D. J. (2004) Cell biology of protein misfolding: The examples of Alzheimer's and Parkinson's diseases. *Nat. Cell Biol. 6*, 1054−1061.

(37) Marshall, K. E., Vadukul, D. M., Dahal, L., Theisen, A., Fowler, M. W., Al-Hilaly, Y., Ford, L., Kemenes, G., Day, I. J., Staras, K., and Serpell, L. C. (2016) A critical role for the self-assembly of Amyloid-β1−42 in neurodegeneration. *Sci. Rep. 6*, 1−13.

(38) Tyedmers, J., Madariaga, M. L., and Lindquist, S. (2008) Prion switching in response to environmental stress. *PLoS Biol. 6*, 2605−2613.

(39) van Leeuwen, F. W., and Kampinga, H. H. (2018) Heat shock proteins and protein quality control in Alzheimer's disease, in *The Molecular and Cellular Basis of Neurodegenerative Diseases* (Wolfe, M. S., Ed.), pp 269−298, Elsevier.

(40) Keller, J. N., Hanni, K. B., and Markesbery, W. R. (2000) Impaired proteasome function in Alzheimer's disease. *J. Neurochem. 75*, 436−439.

(41) Cohen, S. I. A., Linse, S., Luheshi, L. M., Hellstrand, E., White, D. A., Rajah, L., Otzen, D. E., Vendruscolo, M., Dobson, C. M., and Knowles, T. P. J. (2013) Proliferation of amyloid-β42 aggregates occurs through a secondary nucleation mechanism. *Proc. Natl. Acad. Sci. U. S. A. 110*, 9758−9763.

(42) Lashuel, H. A., Overk, C. R., Oueslati, A., and Masliah, E. (2013) The many faces of α-synuclein: From structure and toxicity to therapeutic target. *Nat. Rev. Neurosci. 14*, 38−48.

(43) Conway, K. A., Lee, S.-J., Rochet, J.-C., Ding, T. T., Williamson, R. E., and Lansbury, P. T. (2000) Acceleration of oligomerization, not fibrillization, is a shared property of both alpha -synuclein mutations linked to early-onset Parkinson's disease: Implications for pathogenesis and therapy. *Proc. Natl. Acad. Sci. U. S. A. 97*, 571−576.

(44) Fredenburg, R. A., Rospigliosi, C., Meray, R. K., Kessler, J. C., Lashuel, H. A., Eliezer, D., and Lansbury, P. T. (2007) The impact of the E46K mutation on the properties of α-synuclein in its monomelic and oligomeric states. *Biochemistry 46*, 7107−7118.

(45) Lemkau, L. R., Comellas, G., Kloepper, K. D., Woods, W. S., George, J. M., and Rienstra, C. M. (2012) Mutant protein A30P α-synuclein adopts wild-type fibril structure, despite slower fibrillation kinetics. *J. Biol. Chem. 287*, 11526−11532.

(46) Li, J., Uversky, V. N., and Fink, A. L. (2001) Effect of familial Parkinson's disease point mutations A30P and A53T on the structural properties, aggregation, and fibrillation of human α-synuclein. *Biochemistry 40*, 11604−11613.

(47) Lashuel, H. A., Petre, B. M., Wall, J., Simon, M., Nowak, R. J., Walz, T., and Lansbury, P. T. (2002) A-Synuclein, Especially the Parkinson'S Disease-Associated Mutants, Forms Pore-Like Annular and Tubular Protofibrils. *J. Mol. Biol. 322*, 1089−1102.

(48) Flagmeier, P., Meisl, G., Vendruscolo, M., Knowles, T. P. J., Dobson, C. M., Buell, A. K., and Galvagnion, C. (2016) Mutations associated with familial Parkinson's disease alter the initiation and amplification steps of α-synuclein aggregation. *Proc. Natl. Acad. Sci. U. S. A. 113*, 10328−10333.

(49) Dixon, C., Mathias, N., Zweig, R. M., Davis, D. A., and Gross, D. S. (2005) alpha-synuclein targets the plasma membrane via the secretory pathway and induces toxicity in yeast. *Genetics 170*, 47−59.

(50) Jo, E., Fuller, N., Rand, R. P., St George-Hyslop, P., and Fraser, P. E. (2002) Defective membrane interactions of familial Parkinson's disease mutant A30P α-Synuclein. *J. Mol. Biol. 315*, 799−807.

(51) Laine, R. F., Sinnige, T., Ma, K. Y., Haack, A. J., Poudel, C., Gaida, P., Curry, N., Perni, M., Nollen, E. A. A., Dobson, C. M., Vendruscolo, M., Kaminski Schierle, G. S., and Kaminski, C. F. (2019) Fast fluorescence lifetime imaging reveals the aggregation processes of α-synuclein and polyglutamine in aging Caenorhabditis elegans. *ACS Chem. Biol. 14*, 1628−1636.

(52) Chernoff, Y. O., Derkach, I. L., and Inge-Vechtomov, S. G. (1993) Multicopy SUP35 gene induces de-novo appearance of psi-like factors in the yeast Saccharomyces cerevisiae. *Curr. Genet. 24*, 268.

(53) Harvey, Z. H., Chen, Y., and Jarosz, D. F. (2018) Protein-based inheritance: epigenetics beyond the chromosome. *Mol. Cell 69*, 195−202.

(54) Alberti, S., Halfmann, R., King, O., Kapila, A., and Lindquist, S. (2009) A Systematic Survey Identifies Prions and Illuminates Sequence Features of Prionogenic Proteins. *Cell 137*, 146.

(55) Sondheimer, N., and Lindquist, S. (2000) Rnq1: An epigenetic modifier of protein function in yeast. *Mol. Cell 5*, 163−172.

(56) Derkatch, I. L., Chernoff, Y. O., Kushnirov, V. V., Inge-Vechtomov, S. G., and Liebman, S. W. (1996) Genesis and variability of [PSI] prion factors in Saccharomyces cerevisiae. *Genetics 144*, 1375−1386.

(57) Liebman, S. W., and Chernoff, Y. O. (2012) Prions in yeast. *Genetics 191*, 1041−1072.

(58) Derkatch, I. L., Bradley, M. E., Hong, J. Y., and Liebman, S. W. (2001) Prions Affect the Appearance of Other Prions: The Story of [PIN] University of Illinois at Chicago. *Cell 106*, 171−182.

(59) Huang, V. J., Stein, K. C., and True, H. L. (2013) Spontaneous Variants of the [RNQ+] Prion in Yeast Demonstrate the Extensive Conformational Diversity Possible with Prion Proteins. *PLoS One 8*, 1−14.

(60) McGlinchey, R. P., Kryndushkin, D., and Wickner, R. B. (2011) Suicidal [PSI+] is a lethal yeast prion. *Proc. Natl. Acad. Sci. U. S. A. 108*, 5337−5341.

(61) Nourseothricin Additional Information and List of Selectable Organisms, https://www.jenabioscience.com/images/b3e879b381/Nourseothricin_information.pdf (accessed 2/25/2020).